Journal of Thermal Analysis and Calorimetry, Vol. 85 (2006) 1, 119–124

THERMAL, SPECTRAL AND AFM STUDIES OF CALCIUM SILICATE HYDRATE-POLYMER NANOCOMPOSITE MATERIAL

S. C. Mojumdar[1*], *L. Raki*[1], *N. Mathis*[2], *K. Schimdt*[2] *and S. Lang*[3]

[1]Institute for Research in Construction, National Research Council Canada, M-20, 1200 Montreal Road, Ottawa, Ontario K1A 0R6, Canada
[2]Mathis Instruments Ltd., 21 Alison Blvd., Fredericton, NB E3C 2N5, Canada
[3]Steacie Institute for Molecular Sciences, National Research Council, Ottawa, ON, K1A OR6, Canada

A non-ionic polymer (poly(vinyl alcohol) (PVA)) has been incorporated into the inorganic layers of calcium silicate hydrate (C–S–H) during precipitation of quasicrystalline C–S–H from aqueous solution. C–S–H and a C–S–H-polymer nanocomposite (C–S–HPN) material were synthesized and characterized by X-ray fluorescence (XRF), energy dispersive spectroscopy (EDS), ^{29}Si magic angle spinning nuclear magnetic resonance (^{29}Si MAS NMR) and ^{13}C cross-polarization nuclear magnetic resonance (^{13}C CP NMR) spectroscopy, atomic force microscopy (AFM), thermal conductivity, thermogravimetric analysis (TG) and differential thermal analysis (DTA). Thermal conductivity of PVA, C–S–H and C–S–HPN material was studied in the temperature range 25–50°C. C–S–HPN materials exhibited the highest thermal conductivity at 25 and 50°C. The thermal conductivity increases from 25 to 50°C are 7.03, 17.46 and 14.85% for PVA, C–S–H and C–S–HPN material, respectively. Three significant decomposition temperature ranges were observed on the TG curve of C–S–HPN material.

Keywords: *AFM, C–S–H, C–S–HPN nanocomposites, DTA, NMR spectroscopy, PVA, TG, thermal conductivity*

Introduction

Thermal performance of materials is crucial in many industries, ranging from pharmacy, battery and aerospace and electronics to the construction industries. As a result, thermal characterization of nanocomposite materials is very important in developing new materials and optimizing materials' performance and reliability. Therefore, as key parameters of thermal characterization; thermal conductivity, thermogravimetric analysis and differential thermal analysis are of considerations at all levels when thermal engineers design for optimum thermal stability, heat dissipation, bonding and homogeneity. Consequently, it is highly desired to use efficient, effective testing methods to measure the thermal properties of nanocomposite materials [1, 2]. Thermal conductivity is the time rate of steady state heat flow through a unit area of a homogeneous material induced by a unit temperature gradient in a direction perpendicular to that unit area, in W m^{-1} K^{-1}. The measurement of thermal conductivity involves a set of parameters that are common to different techniques and methodologies. Aside from variations due to the nature and type of samples, all methodologies require determination of the actual amount of heat transferred through the sample along and perpendicular to the heat flow path in a given thermal environment. Conductivity, as opposed to conductance, provides dimensional attributes to the calculated value. Thus, thermal conductivity is related to a material property that denotes a rate process of heat transfer. Since diffusion is the primary mode of heat propagation in a solid body, thermal conductivity is a function of diffusivity, density and heat capacity [3]. Thermal conductivity, thermal diffusivity, heat flow rate, heat transfer value, thermal stability, Fourier-transform infrared (FTIR) and/or AFM results are very important parameters for the characterization of materials ranging from gaseous through liquid to solid. Therefore, it is not surprising that many authors studied the thermal properties including thermal stability, thermal conductivity, together with XRF, spectral and microscopic studies to characterize various materials [1–10].

Nanocomposites are a new class of composites, that are particle-filled polymers for which at least one dimension of the dispersed particles is in the nanometer range. Three types of nanocomposites, depending on how many dimensions of the dispersed particles are in the nanometer range can be distinguished [11]. Particles with three dimensions in the order of nanometers are typically isodimensional, such as spherical silica nanoparticles obtained by in situ sol–gel methods [12, 13] or by polymerization promoted directly from their surface [13, 14]. They also include semiconductor nanoclusters [15] and others [13]. Nanotubes or whiskers (with two dimensions in the nanometer scale and the third forming a larger elongated structure), for example, carbon nanotubes [16] or cellulose whis-

* Author for correspondence: Subhash.Mojumdar@nrc-cnrc.gc.ca

1388–6150/$20.00

Akadémiai Kiadó, Budapest, Hungary
Springer, Dordrecht, The Netherlands

kers [17, 18], are extensively studied as reinforcing phases yielding materials with exceptional properties. The third type of nanocomposites is characterized by only one dimension in the nanometer range. This family of composites is referred to as polymer-layered crystal nanocomposites. Three main types of composites may be obtained when a layered structure is associated with a polymer [11]. If the polymers are unable to intercalate between the layered sheets, a phase-separated composite is obtained, whose properties stay in the same range as traditional microcomposites. Beyond this classical family of composites, two types of nanocomposites can be distinguished. An 'intercalated' structure in which a single (and sometimes more than one) extended polymer chain is intercalated between the inorganic layers resulting in a well-ordered multilayer morphology built up with alternating polymeric and inorganic layers. When the layers are completely and uniformly dispersed in a continuous polymer matrix, an 'exfoliated or delaminated' structure is obtained. Other intermediate organizations can exist presenting both intercalation and exfoliation, where a broadening of the diffraction peak is often observed [11].

Nanocomposites are reported to promote thermal [19, 20], mechanical [21], molecular barriers [22], flame retardant behavior [23–30] and corrosion protection properties [31–33]. Therefore, the systematic investigation and the reaction possibility of PVA with synthetic C–S–H at low Ca/Si ratio (0.7) as well as the characterization of the nanocomposite by thermal conductivity, thermoanalytical and other nanotechnological methods are the main interests of this contribution.

Experimental

Synthesis of C–S–HPN materials

C–S–H and C–S–HPN material (CSH–PVA (0.7–0.15)) with PVA content of 0.15 g/g Ca salt, were synthesized by gradually adding calcium nitrate solution (1 mol L^{-1}) with continual stirring under nitrogen to sodium silicate solution, which was pre-dissolved with PVA (only for the synthesis of C–S–HPN material) in CO_2-free de-ionized water. The amount of $Ca(NO_3)_2{\cdot}4H_2O$ and $Na_2SiO_3{\cdot}9H_2O$ were calculated to maintain the initial Ca/Si molar ratio 7.0 for C–S–H and C–S–HPN material. The pH value was kept between 13.1–13.4 by adding NaOH solution (4.0 M) during the precipitation of C–S–H. After aging the suspension at 60°C for seven days with stirring, the precipitate was separated by vacuum filtration and washed with CO_2-free de-ionized water to remove sodium and nitrate ions and any residual PVA. The precipitates were then washed with acetone and dried at 60°C in a vacuum oven for 7 days.

Methods

The Mathis TC-01 system, which employs the modified hot wire technology, was used to perform the thermal conductivity measurements. Samples were tested as they were synthesized and purified without additional sample preparation. During all measurements, a 652 g mass was placed on the top of the sample to ensure a good contact between the sample and sensor. The test times utilized were 2.3–5.0 s.

Thermal analysis on powder samples (~20 mg) were carried out using a simultaneous SDT Q600 T.A.I. instrument at 10°C min^{-1} from room temperature (*RT*) to 1000°C under nitrogen atmosphere using a flowing rate 100 mL min^{-1}. EDS measurements were conducted using a Cambridge Systems Stereoscan 250 Instrument equipped with an Oxford Instruments Inca 200 EDS. AFM images were acquired on a Jeol SPM 5200. The system was used in the non-contact AC Mode using a silicon cantilever with a resonance frequency of approximately 170 kHz and a spring constant of 40 N m^{-1}.

^{29}Si MAS NMR spectra were recorded at 39.7 MHz, on a TecMag Apollo spectrometer using a 7 mm Doty probe. Chemical shifts are reported relative to an external tetramethylsilane reference sample. Samples were spun in 7 mm zirconia rotors at 4 kHz, and a 7 μs 90° pulse was used, on both spectrometers. ^{13}C CP NMR spectra were acquired on a Bruker Avance 200 spectrometer. Samples were packed in 7 mm zirconia rotors and spun at 4 kHz. Commercial MAS probes provided by Bruker and Chemmagnetics were used. XRF analysis was performed on a Bruker AXS S4 Pioneer automated XRF machine and analyzed for all elements as oxides.

Results and discussion

Analysis

The compositions of the C–S–H and C–S–HPN material were confirmed by XRF and EDS analysis. The EDS analysis was carried out on several different zones of C–S–H and C–S–HPN material. The composition of C–S–H and C–S–HPN material confirmed the theoretical expectation (Ca/Si=0.7).

^{13}C CP NMR and ^{29}Si MAS NMR spectra

The ^{13}C CP NMR spectra of C–S–HPN material (Fig. 1) have been compared to dry pure commercial PVA spectra [34]. The spectra of pure PVA is similar to that of atactic (at-) PVA and show the methylene signal at 45 ppm. The methine carbon resonances are observed at about 77 (peak I), 71 (peak II) and 65 ppm (peak III). Following previous NMR investigations [34], peaks I and II have been assigned to the mm

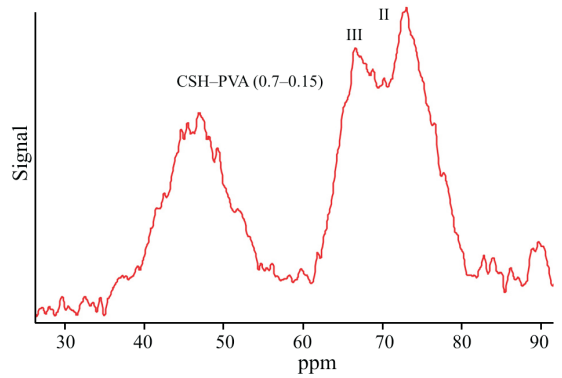

Fig. 1 ^{13}C CP NMR spectra of C–S–HPN material (CSH–PVA (0.7–0.15))

(heterotactic) triads with two intramolecular hydrogen bonds and to the mm and mr (heterotactic) triads with one intramolecular hydrogen bond, respectively, while peak III has been attributed to the mm, mr and rr (syndiotactic) triads (where m and r indicate meso and racemic dyads, respectively) with no intervening intramolecular hydrogen bonds. The spectra of C–S–HPN materials show the methylene signal at 46 ppm and only two methine carbon resonances at about 72 ppm (peak II) and 66 ppm (peak III). The signal at 77 ppm (peak I) [34] has been missing for C–S–HPN material. Comparing the spectra of pure PVA to that of C–S–HPN material clearly shows that the PVA reactions with C–S–H in aqueous media largely disrupts the network of two and one intramolecular hydrogen bonds between hydroxyl groups as a function of the degree of tacticity and the gelation procedure with C–S–H, and promotes the formation of new networks of interchain hydrogen bonds.

The analysis is based on the Q^n classification [35] where Q represents a SiO_4^{4-} unit and the degree of connectivity, n, is related to the oxygen bonds number between the SiO_4^{4-} units. The ^{29}Si MAS NMR spectra of C–S–HPN material are presented in Fig. 2. The ^{29}Si MAS NMR spectra of C–S–H (not shown) and

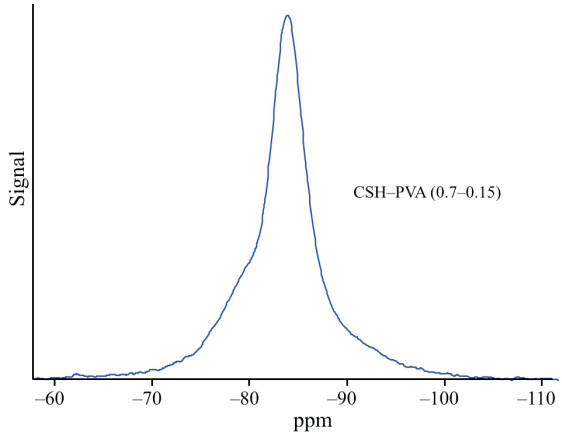

Fig. 2 ^{29}Si MAS NMR spectra of C–S–HPN material (CSH–PVA (0.7–0.15))

C–S–HPN material contain mainly the Q^2 peak at about –84 ppm. However, a weak Q^1 peak or a shoulder is present in all spectra at about –79 ppm [35]. According to the ^{29}Si MAS NMR spectra, it can be concluded that the C–S–H and C–S–HPN materials have the structure similar to that of tobermorite [35].

AFM analysis

AFM analysis was performed on bulk PVA, C–S–H and C–S–HPN material films to study the morphology of pure PVA, C–S–HPN material and C–S–H. Observation of the all materials films was done using AC mode. This AFM mode was chosen to observe the topographical and phase images of the studied materials as well as to illustrate the fundamental use of this AFM mode. Topographical and phase images of PVA, C–S–H and C–S–HPN material, achieved by AFM analysis are presented in Fig. 3. There are significant differences between the topographical and phase images of PVA, C–S–H and C–S–HPN material. Mechanical variation across material surfaces as those between amorphous and crystalline regions are manifested in various AFM images. When PVA polymer was added to inorganic C–S–H layers, crystallites were initiated and grown in the immediate vicinity of the inorganic surface. We believe that this is due to the strong specific interactions between the inorganic surfaces and the polymer. The PVA vinyl alcohol group forms hydrogen bonds with the silicate oxygen, which dominate the cleavage plane of C–S–H. Moreover, due to the atomically smooth C–S–H surface, these specific interactions are expected to force chains to create long adsorbed trains, which in turn will promote a strongly interacting second layer of PVA to crystallize on top of them. Thus, this C–S–H surface epitaxial/nucleating effect can be 'felt' through many layers of polymer, causing a long-range collection and crystallization of PVA from the surface of the silicate. Therefore, these sites tend to act as nucleating sites for the PVA crystallites. Accordingly, scans of the C–S–HPN materials show many more crystallites per area compared to the neat PVA, as all the inorganic silicate fillers nucleate polymer crystallites. The PVA/C–S–H specific interactions decrease the surface energy necessary to create/nucleate a polymer crystal, and thus, the crystalline regions tend to nucleate around the silicate surfaces.

Thermal conductivity

The modified hot wire transient technique was applied to measure the thermal conductivity of the studied samples. This technique can non-destructively and accurately measure the thermal conductivity and thermal effusivity of a material in seconds. The modification

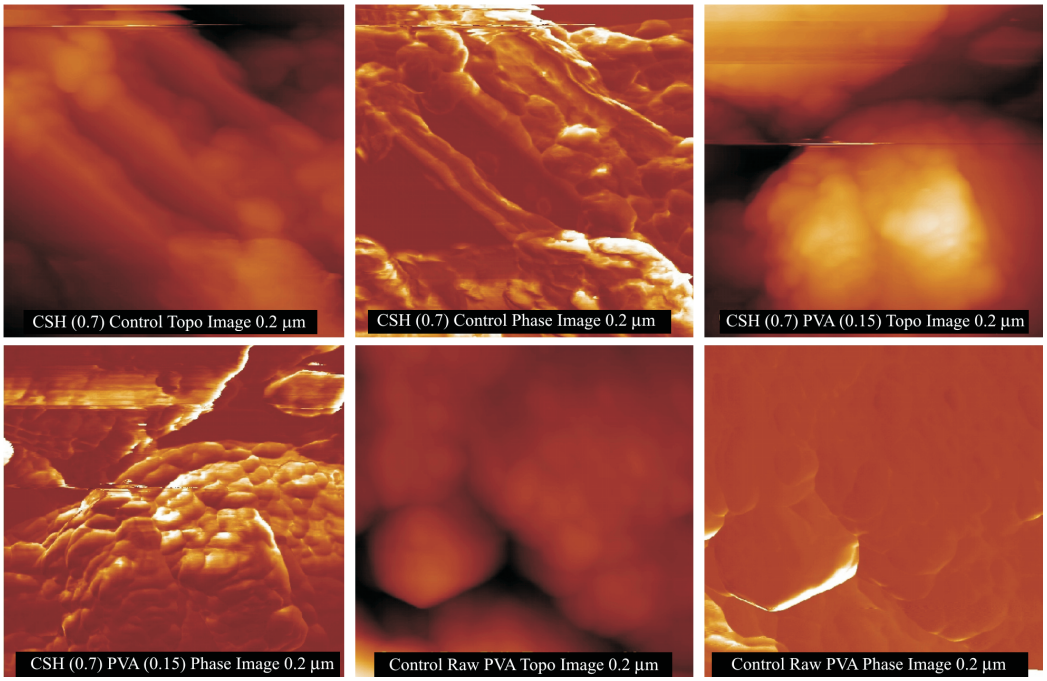

Fig. 3 AFM micrographs of C–S–H, C–S–HPN material and PVA

compared to the hot wire technique is that the heating elements are supported on a backing, which provides mechanical support, electrical insulation, and thermal insulation. Such modification eliminates the intrusive nature of the hot wire technique, thereby allowing solids to be tested without melting or otherwise modifying the sample to conform to the geometry of the test cell.

The measured thermal conductivities of PVA, C–S–H and C–S–HPN material samples at 25 and 50°C are presented in Table 1. The following conclusions can be drawn from the thermal conductivity measurements.

An accuracy of 0.5% or better was observed in the thermal conductivity measurements of each sample, indicating the high reliability of the measurements performed in the study.

An RSD value of 1.5% or better was observed in each set of the measurements, illustrating the high reproducibility of the measurements conducted.

The lowest thermal conductivity at 25°C was observed for C–S–H; however, PVA exhibited the lowest thermal conductivity at 50°C. C–S–HPN material exhibited the highest thermal conductivity in both cases. However, the highest thermal conductivity increase was observed for C–S–H. These observations are due to different conductive capacity of different materials at different temperature. The thermal conductivity increases from 25 to 50°C are 7.03, 17.46 and 14.85% for PVA, C–S–H and C–S–HPN material, respectively.

TG and DTA analysis of C–S–H, PVA and C–S–HPN material

The most important thermoanalytical (TG and DTA) data of C–S–H, C–S–HPN material and PVA are presented in Table 2 and Figs 4 and 5. Figure 4 shows the TG curves of C–S–H, PVA and C–S–HPN material. There are significant differences in the thermal decomposition properties of C–S–H, PVA and C–S–HPN material. C–S–HPN material has exhibited higher thermal stability than the starting materials PVA and C–S–H. In general, three temperature regions on the TG curve of C–S–HPN material were observed:

- *RT*–250°C: this is the region of C–S–H decomposition [36–53] due to loss of molecular water with DTA peaks at 71–134°C. In the case of C–S–HPN material, the decomposition temperature (T_d) in this region is variable depending on the synthesis and material compositions.

Table 1 Measured thermal conductivities of C–S–H, C–S–HPN material and PVA

Sample	Average of the measured k/W m^{-1} K^{-1}		Increase from 25 to 50°C/%	RSD/%	
	25°C	50°C		25°C	50°C
PVA	0.1063	0.11375	7.03	0.81	0.13
C–S–HPN material	0.1650	0.1895	14.85	0.39	0.11
C–S–H	0.1012	0.1189	17.46	4.61	0.17

*k –thermal conductivity

Table 2 Summary of thermal analysis data for C–S–H, PVA and C–S–HPN materials

Material	T_d/°C	DTA peak/°C
C–S–H	250 over 550	71, 693
C–S–H–PVA (0.7–0.15)	250, 550 over 550	134, 356, 701
PVA	250, 370, 500	57, 283, 459

T_d=decomposition temperature

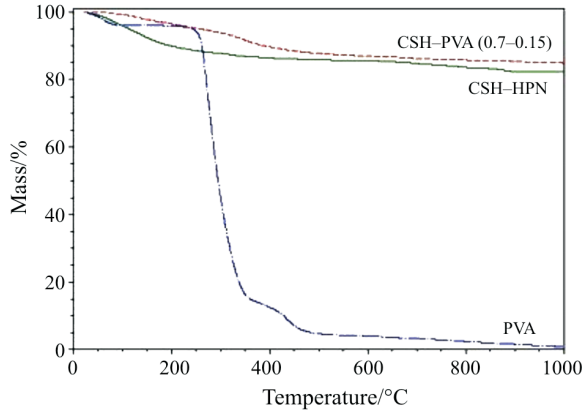

Fig. 4 TG curves of C–S–H, PVA and C–S–HPN material with different polymer contents

- 250–550°C: this temperature region is attributed mainly to the polymeric material decomposition [36–53]. DTA curves for C–S–HPN material as well as PVA exhibit DTA peaks at the temperature range 283–459°C (Table 2, Fig. 5). The shift of DTA peak to the higher temperature in C–S–HPN material compared to pure PVA and C–S–H is due to the improved thermal stability of C–S–HPN material.
- Over 550°C: this temperature region is characteristic for structural water and $CaCO_3$ decomposition [36–53]. The atmospheric moisture and CO_2 causes the formation of $Ca(OH)_2$ and $CaCO_3$.

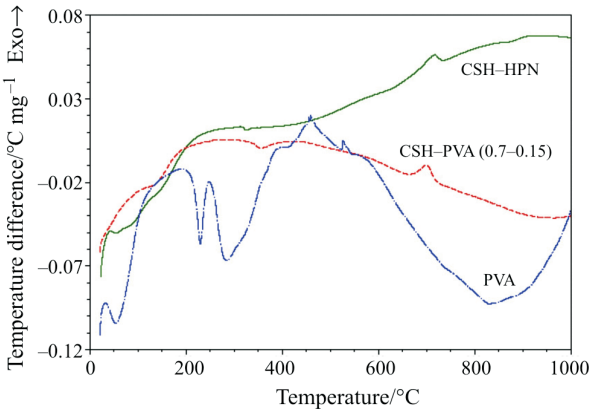

Fig. 5 DTA curves of C–S–H, PVA and C–S–HPN material (PVA=0.15 g/g Ca salt)

Conclusions

New calcium silicate hydrate/poly(vinyl alcohol) nanocomposite (C–S–HPN) materials have been synthesized and characterized. Synthetic C–S–H and C–S–HPN materials were analyzed using XRF, EDS, AFM, TG, DTA and thermal conductivity. Significant differences in the morphologies of C–S–H, PVA and C–S–HPN material have been observed in AFM micrographs. The influence of the material composition on the thermal decomposition of C–S–HPN material along with the pure PVA and synthetic C–S–H has been studied by TG and DTA. Three significant decomposition temperature regions were observed in the TG curves of C–S–HPN material, corresponding to the decomposition temperature of C–S–H structure, polymeric entities, and structural water and $CaCO_3$. The lowest thermal conductivity at 25°C was observed for C–S–H. On the other hand, PVA exhibited the lowest thermal conductivity at 50°C. C–S–HPN material exhibited the highest thermal conductivity not only at 25 but also at 50°C.

This study leads to new routes for developing new cement-based nanocomposite materials for future potential applications in the construction field, such as coatings for corrosion protection, for fire retardancy and others. A systematic investigation to understand the effect of PVA molecules intercalation on Ca/Si ratio of C–S–HPN material by means of TEM, XPS, DMA and TMA will be discussed in a future article.

Acknowledgements

The authors would like to thank Jim Margeson for AFM and XRF measurements.

References

1 S. C. Mojumdar and L. Raki, J. Therm. Anal. Cal., 82 (2005) 89.
2 S. C. Mojumdar and L. Raki, J. Therm. Anal. Cal., OnlineFirst, DOI: 10.1007/s10973-005-7353-9.
3 X. Qiu, N. Mathis and K. Schimdt, Thermochim. Acta, in press.
4 B. Chowdhury and S. C. Mojumdar, J. Therm. Anal. Cal., 81 (2005) 179.
5 S. C. Mojumdar, J. Therm. Anal. Cal., 64 (2001) 1133.
6 B. Chowdhury, J. Therm. Anal. Cal., 78 (2004) 215.
7 L. Sun, J. E. S. Venart and R. C. Prasad, Int. J. Thermophys., 23 (2002) 357.
8 F. Su and R. C. Prasad, Int. Commun. Heat Mass, 30 (2003) 603.
9 S. C. Mojumdar and L. Raki, J. Therm. Anal. Cal., accepted.
10 I. Janotka and S. C. Mojumdar, J. Therm. Anal. Cal., 81 (2005) 197.

11 M. Alexandre and P. Dubois, Mater. Sci. Eng., 28 (2000) 1.
12 J. E. Mark, Polym. Eng. Sci., 36 (1996) 2905.
13 E. Reynaud, C. Gauthier and J. Perez, Rev. Metall./Cah. Inf. Tech., 96 (1999) 169.
14 T. Von Werne and T. E. Patten, J. Am. Chem. Soc., 121 (1999) 7409.
15 N. Heron and D. L. Thorn, Adv. Mater., 10 (1998) 1173.
16 P. Cavert, Potential Application of Nanotubes, in Carbon Nanotubes, CRC Press, T. W. Ebbesen (Ed.), Boca Raton, FL 1997, pp. 277–292.
17 V. Favier, G. R. Canova, S. C. Shrivastava and J. Y. Cavaille, Polym. Eng. Sci., 37 (1997) 1732.
18 L. Chazeau, J. Y. Cavalle, G. Canova, R. Dendievel and B. Boutherin, J. Appl. Polym. Sci., 71 (1999) 1797.
19 M. Zanetti, P. Bracco and L. Costa, Polym. Degrad. Stab., 85 (2004) 657.
20 H.-L. Tyan, Y.-C. Liu and K.-H. Wei, Chem. Mater., 11 (1999) 1942.
21 Z. Wang and T. J. Pinnavaia, Chem. Mater., 10 (1998) 3769.
22 J. Liu, Y. Gao, F. Wang and W. Ming, J. Appl. Polym. Sci., 75 (2000) 384.
23 J. W. Gilman, Appl. Clay Sci., 15 (1999) 31.
24 J. W. Gilman, C. L. Jackson, A. B. Morgan, J. R. Hayyis, E. Manias, E. P. Giannelis, M. Wuthenow, D. Hilton and S. H. Philips, Chem. Mater., 12 (2000) 1866.
25 D. Porter, E. Metcalfe and M. J. K. Thomas, Fire Mater., 24 (2000) 45.
26 J. Wang, J. Dua, J. Zhu and C. A. Wilkie, Polym. Degrad. Stab., 77 (2002) 249.
27 M. Zanetti, G. Camino, D. Canavese, A. B. Morgan, F. J. Lamelas and C. A. Wilkie, Chem. Mater., 14 (2002) 189.
28 M. Zanetti, T. Kashiwagi, L. Falqui and G. Camino, Chem. Mater., 14 (2002) 881.
29 J. Zhu, P. Start, K. A. Mauritz and C. A. Wilkie, Polym. Degrad. Stab., 77 (2002) 253.
30 J. Zhu, F. Uhl, A. B. Morgan and C. A. Wilkie, Chem. Mater., 13 (2001) 4649.
31 J. M. Yeh, S. J. Liou, C. Y. Lai, P. C. Wu and T. Y. Tsai, Chem. Mater., 13 (2001) 1131.
32 J. M. Yeh, C. L. Chen, Y. C. Chen, C. Y. Ma, K. R. Lee, Y. Wei and S. Li, Polymer, 43 (2002) 2729.
33 J. M. Yeh, S. J. Liou, C. Y. Lin, C. Y. Cheng, Y. W. Chang and K. R. Lee, Chem. Mater., 14 (2002) 154.
34 M. Kobayashi, I. Ando, T. Ishii and S. Amiya, J. Mol. Struct., 440 (1998) 155.
35 Z. H. Zanni, R. Rassem-Bertolo, S. Masse, L. Fernandez, P. Nieto and B. Bresson, Magnet. Resonan. Imag., 14 (1996) 827.
36 A. A. Ibrahim, H. H. ElSersy and M. F. Abadir, J. Therm. Anal. Cal., 76 (2004) 713.
37 S. C. Mojumdar and L. Raki, J. Therm. Anal. Cal., accepted.
38 S. C. Mojumdar and L. Raki, Preparation and Properties of Calcium Silicate Hydrate Polymer Nanocomposite, 107th American Ceramics Society Annual Meeting, Exposition and Technology Fair, April 10–13, 2005, Baltimore, MD, USA.
39 S. C. Mojumdar and L. Raki, Ceram. Trans. (Ceram. Nanomat. Nanotech. IV), in press (2006).
40 J. Dweck, P. F. Ferreira da Silva, R. Silva Aderne, P. M. Büchler and F. K. Cartledge, J. Therm. Anal. Cal., 71 (2003) 821.
41 S. C. Mojumdar, B. Chowdhury, K. G. Varshney and K. Mazanec, J. Therm. Anal. Cal., 78 (2004) 135.
42 T. Lan, P. D. Kaviratna and T. J. Pinnavaia, Chem. Mater., 6 (1994) 573.
43 I. Odler, 2000, Special Inorganic Cement, Capter 13.3, MDF cement, London, New York: E and F. N. Spon, pp. 1–395.
44 B. Chowdhury, J. Therm. Anal. Cal., 78 (2004) 215.
45 S. C. Mojumdar, Res. J. Chem. Environ., 9 (2005) 23.
46 S. C. Mojumdar, J. Therm. Anal. Cal., 64 (2001) 1133.
47 S. C. Mojumdar, Challeng, Coord. Chem. New Century, 5 (2001) 453.
48 I. Janotka and L'. Krajči, Bull. Mater. Sci., 23 (2000) 521.
49 H. F. W. Taylor, Cement Chemistry, 2nd Edn. Thomas Telford Publ., London, UK 1998.
50 I. Janotka, L'. Krajči, A. Ray and S. C. Mojumdar, Cem. Concr. Res., 33 (2003) 489.
51 I. Janotka and S. C. Mojumdar, Sol. Stat. Phenom., 90–91 (2003) 309.
52 I. Janotka, T. Nürnbergerová and L. Nad, Magaz. Concr. Res., 52 (2000) 399.
53 Y. H. Yu, C. Y. Lin, J. M. Yeh and W. H. Lin, Polymer, 44 (2003) 3553.

DOI: 10.1007/s10973-005-7354-8